Long-range ferromagnetic correlations between Anderson impurities in a semiconductor host

N. Bulut[1,2], K. Tanikawa[1], S. Takahashi[1], and S. Maekawa[1,2]
[1] *Institute for Materials Research, Tohoku University, Sendai 980-8577, Japan*
[2] *CREST, Japan Science and Technology Agency (JST), Kawaguchi, Saitama 332-0012, Japan*
(Dated: November 22, 2006)

We study the two-impurity Anderson model for a semiconductor host using the quantum Monte Carlo technique. We find that the impurity spins exhibit ferromagnetic correlations with a range which can be much more enhanced than in a half-filled metallic band. In particular, the range is longest when the Fermi level is located above the top of the valence band and decreases as the impurity bound state becomes occupied. Comparisons with the photoemission and optical absorption experiments suggest that this model captures the basic electronic structure of $Ga_{1-x}Mn_xAs$, the prototypical dilute magnetic semiconductor (DMS). These numerical results might also be useful for synthesizing DMS or dilute-oxide ferromagnets with higher Curie temperatures.

PACS numbers: 75.50.Pp, 75.30.Hx, 75.40.Mg, 71.55.-i

The discovery of ferromagnetism in alloys of III-V semiconductors with Mn started an intense research activity in the field of dilute magnetic semiconductors (DMS) [1, 2, 3]. Room-temperature ferromagnetism in DMS would be a significant development for spintronics device applications. In this respect, it is important to understand the nature of the correlations which develop between magnetic impurities in semiconductors and how they differ from that in a metallic host. With this purpose, we present exact numerical results on the two-impurity Anderson model for a semiconductor host.

In order to study the multiple charge states of Au impurities in Ge, the single-impurity Anderson model of a metallic host was extended to the case of a semiconductor host using the Hartree-Fock (HF) approximation [4]. After the discovery of DMS, the magnetic properties of this model were addressed within HF [5, 6]. It was shown that long-range ferromagnetic (FM) correlations develop between Anderson impurities in a semiconductor when the Fermi level is located between the top of the valence band and the impurity bound state (IBS), as illustrated in Fig. 1. The FM interaction between the impurities is mediated by the impurity-induced polarization of the valence electron spins, which are antiferromagnetically coupled to the impurity moments. Within HF, the impurity-host hybridization also induces host split-off states at the same energy as the IBS. When the split-off state becomes occupied, the spin polarizations of the valence band and of the split-off state cancel. This causes the long-range FM correlations between the impurities to vanish. Within the context of DMS, the Anderson Hamiltonian for a semiconductor host was also considered by Krstajić *et al.* [7], and it was shown that an FM interaction is generated between the impurities due to kinematic exchange. In addition, this model was studied within HF for investigating the multiple charge and spin states of transition-metal atoms in hemoprotein [8].

In this paper, we present quantum Monte Carlo (QMC) data on the two-impurity Anderson model for a semiconductor host and make comparisons with the HF results. We find that in a semiconductor the nature of the magnetic correlations between the impurities is different than in a metallic host. In particular, the impurities exhibit long-range FM correlations when the Fermi level is located above the top of the valence band, and the FM correlations weaken as the IBS becomes occupied in agreement with HF [5, 6]. Comparisons with the photoemission and optical absorption experiments suggest that this model captures the basic electronic structure of $Ga_{1-x}Mn_xAs$. These numerical results outline the parameter regime which yields the longest-range FM correlations, and this information might be useful for synthesizing DMS or dilute-oxide ferromagnets with higher Curie temperatures.

The two-impurity Anderson model for a semiconductor host is defined by

$$H = \sum_{\mathbf{k},\alpha,\sigma} (\varepsilon^{\alpha}_{\mathbf{k}} - \mu) c^{\dagger}_{\mathbf{k}\alpha\sigma} c_{\mathbf{k}\alpha\sigma} + \sum_{\mathbf{k},i,\alpha,\sigma} (V_{\mathbf{k}i} c^{\dagger}_{\mathbf{k}\alpha\sigma} d_{i\sigma} + \text{H.c.}) + E_d \sum_{i,\sigma} d^{\dagger}_{i\sigma} d_{i\sigma} + U \sum_{i} n_{id\uparrow} n_{id\downarrow}, \quad (1)$$

where $c^{\dagger}_{\mathbf{k}\alpha\sigma}$ ($c_{\mathbf{k}\alpha\sigma}$) creates (annihilates) a host electron with wavevector $\mathbf{k}$ and spin σ in the valence ($\alpha = v$) or conduction ($\alpha = c$) band, $d^{\dagger}_{i\sigma}$ ($d_{i\sigma}$) is the creation (annihilation) operator for a localized electron at impurity site i, and $n_{id\sigma} = d^{\dagger}_{i\sigma} d_{i\sigma}$. The hybridization matrix element is $V_{\mathbf{k}j} = V \exp(i\mathbf{k} \cdot \mathbf{R}_j)$, where $\mathbf{R}_j$ is the coordinate of the impurity site j. As usual, E_d is the d-level energy, U is the onsite Coulomb repulsion, and μ the chemical potential. The valence and the conduction bands have the forms $\varepsilon^{v}_{\mathbf{k}} = -D\left(k/k_0\right)^2$ and $\varepsilon^{c}_{\mathbf{k}} = D\left(k/k_0\right)^2 + \Delta_G$, respectively (Figure 1). Here, D is the bandwidth, k_0 is the maximum wavevector and Δ_G is the semiconductor gap. In this paper, we consider a two-dimensional semiconductor host with a constant density of states $\rho_0 = k_0^2/(4\pi D)$.

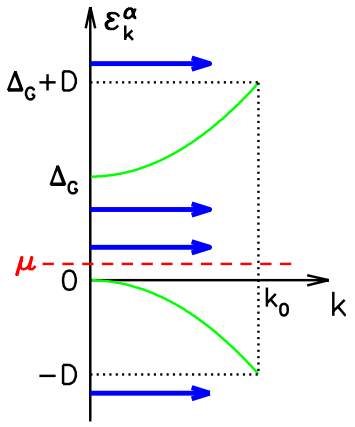

FIG. 1: (color online) Schematic drawing of the semiconductor host bands ε_k^α (solid curves) and the impurity bound states (thick arrows) obtained within HF. The dashed line denotes the chemical potential μ.

We find similar results for the three-dimensional case [9]. We determine the energy scale by setting $D = 12.0$. In addition, we use $U = 4.0$ and $E_d = \mu - U/2$ (the symmetric case), so that the impurity sites develop large moments. We note that this Hamiltonian is particle-hole symmetric with respect to half-filling at $\mu = \Delta_G/2$. For the DMS materials, it is estimated that $\Delta_G/D \approx 0.1$ to 0.2. We report results for $\Delta_G = 2.0$, values of the hybridization parameter $\Delta \equiv \pi\rho_0 V^2$ ranging from 1.0 to 4.0, and inverse temperature $\beta \equiv 1/T$ from 4 to 32. In order to study the evolution of the magnetic correlations as we go from a metallic to a semiconductor host, we will present results for μ from $-D/2$ to $\Delta_G/2$.

The numerical results presented here were obtained with the Hirsch-Fye quantum Monte Carlo technique [10]. In the following, we will first present results on the impurity equal-time magnetic correlation function $\langle M_1^z M_2^z\rangle$, where $M_i^z = n_{id\uparrow} - n_{id\downarrow}$ is the impurity magnetization operator. Next, we will present results on the impurity single-particle spectral weight $A(\omega) = -(1/\pi)\mathrm{Im}\, G_{ii}^\sigma(\omega)$, which is obtained with the maximum-entropy analytic continuation technique [13] from the QMC data on the impurity Green's function

$$G_{ii}^\sigma(\tau) = -\langle T_\tau\, d_{i\sigma}(\tau) d_{i\sigma}^\dagger(0)\rangle. \qquad (2)$$

Here, T_τ is the Matsubara time-ordering operator and $d_{i\sigma}(\tau) = e^{H\tau} d_{i\sigma} e^{-H\tau}$. Since the maximum-entropy procedure requires QMC data with very good statistics, our results on $A(\omega)$ will be limited to the high-temperature $\beta = 8$ case. For lower T, we will discuss QMC results on the impurity occupation number $\langle n_d\rangle = \langle n_{id\uparrow}\rangle + \langle n_{id\downarrow}\rangle$. We will also show data on the zero-frequency inter-impurity magnetic susceptibility defined by

$$\chi_{12}(\omega = 0) = \int_0^\beta d\tau \langle M_1(\tau) M_2(0)\rangle. \qquad (3)$$

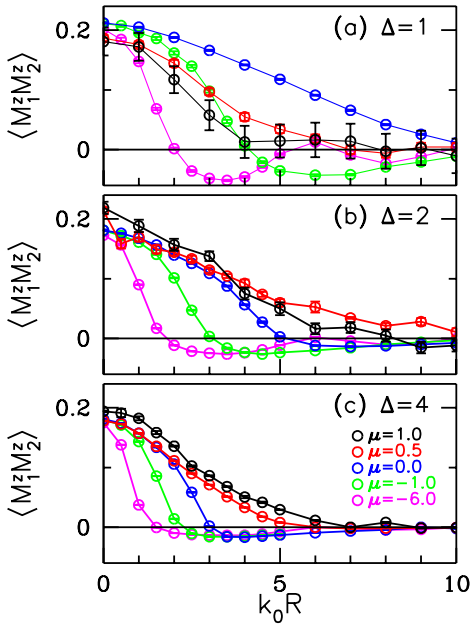

FIG. 2: (color online) $\langle M_1^z M_2^z\rangle$ vs $k_0 R$ plotted at $\beta = 16$ and various μ for hybridization (a) $\Delta = 1.0$, (b) 2.0, and (c) 4.0.

The following results were obtained using Matsubara time steps $\Delta\tau = 0.125$ and 0.25.

Figures 2(a)-(c) show the impurity magnetic correlation function $\langle M_1^z M_2^z\rangle$ vs $k_0 R$, where $R = |\mathbf{R}_1 - \mathbf{R}_2|$ is the impurity separation, at $\beta = 16$ for μ varying from -6.0 to 1.0. Fig. 2(a) is for hybridization $\Delta = 1.0$. At $\mu = -6.0$, we observe oscillations in the R dependence due to an RKKY-type effective interaction between the impurities. These results are similar to what has been obtained previously with QMC for a half-filled metallic band [10, 11, 12]. The wavelength of the oscillations increases when μ moves to -1.0, because of the shortening of the Fermi wavevector. When $\mu = 0.0$, the impurity spins exhibit long-range FM correlations at this temperature. We observe that upon further increasing μ to 0.5 or 1.0, the FM correlations become weaker. This is because the IBS becomes occupied as μ changes from 0.0 to 0.5, as will be seen in Fig. 3(a). In Figs. 2(b) and (c), results on $\langle M_1^z M_2^z\rangle$ are shown for $\Delta = 2.0$ and 4.0, respectively. In Fig. 2(b), we observe that $\langle M_1^z M_2^z\rangle$ has the slowest decay for $\mu = 0.5$, while in Fig. 2(c) this occurs for $\mu = 1.0$. We find that the impurity occupation $\langle n_d\rangle$ increases between $\mu = 0.5$ and 1.0 for $\Delta = 2.0$ and $\beta = 16$. In addition, for $\Delta = 4.0$ and $\beta = 8$, the maximum-entropy image of $A(\omega)$ shows that the IBS is located at $\omega \approx 1.0$. Hence, we observe that the range of the FM correlations for the semiconductor is determined by the occupation of the IBS in agreement with the HF predictions [5, 6]. In Figs. 2(a)-(c), it is also seen that the range increases with decreasing Δ.

In Figs. 3 and 4, we discuss the $\Delta = 1.0$ case in more

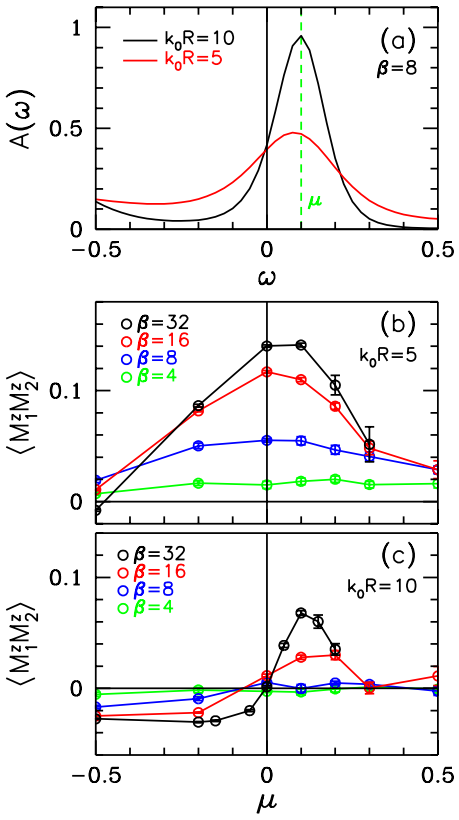

FIG. 3: (color online) (a) Impurity single-particle spectral weight $A(\omega)$ vs ω for $k_0R = 5$ and 10 at $\beta = 8$. Here, the vertical dashed line denotes μ, and the top of the valence band is located at $\omega = 0$. In (b) and (c), $\langle M_1^z M_2^z\rangle$ vs μ is plotted for $k_0R = 5$ and 10, respectively, at various β. These results are for $\Delta = 1.0$.

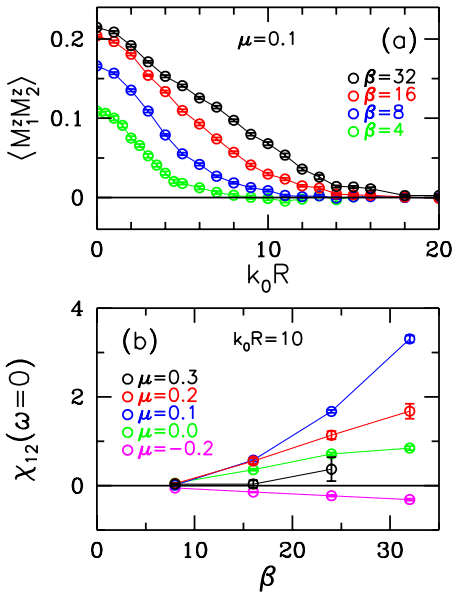

FIG. 4: (color online) (a) $\langle M_1^z M_2^z\rangle$ vs k_0R for $\mu = 0.1$ at various β. (b) Inter-impurity magnetic susceptibility $\chi_{12}(\omega = 0)$ vs β for $k_0R = 10$ at various μ. These results are for $\Delta = 1.0$.

detail. In Fig. 3(a), the impurity spectral weight $A(\omega)$ vs ω is plotted for $\beta = 8$, $\mu = 0.1$, and $k_0R = 5$ and 10. Here, the ω-axis has been shifted so that the top of the valence band is located at $\omega = 0$. For $k_0R = 10$, we observe a peak at $\omega_{BS} \approx 0.1$ in the semiconductor gap, which we identify as the IBS. For $k_0R = 5$, the bound state is broader due to stronger correlations between the impurities. However, we also find that $A(\omega)$ exhibits significant T dependence at $\beta = 8$, and Fig. 3(a) does not yet represent the low-T limit. Next, in Figs. 3(b) and (c), $\langle M_1^z M_2^z\rangle$ evaluated at $k_0R = 5$ and 10 is plotted as a function of μ. Fig. 3(b) shows that, at low T for $k_0R = 5$, $\langle M_1^z M_2^z\rangle$ decreases when $\mu \gtrsim 0.25$. For this value of k_0R and $\beta = 32$, we find that the impurity occupation $\langle n_d\rangle$ develops a step discontinuity at $\mu \approx 0.25$, which is consistent with the decrease of $\langle M_1^z M_2^z\rangle$ when $\mu \gtrsim 0.25$. For $k_0R = 10$ and $\beta = 32$, both $\langle M_1^z M_2^z\rangle$ and $\langle n_d\rangle$ exhibit significant T dependence in the vicinity of the semiconductor gap edge. These results show that $\langle M_1^z M_2^z\rangle$ depends strongly on the value of μ.

Figure 4(a) shows the temperature dependence of $\langle M_1^z M_2^z\rangle$ vs k_0R for $\mu = 0.1$. We observe that, at $\beta = 32$, the range of the FM correlations is enhanced by about an order of magnitude with respect to that in a half-filled metallic band. In Fig. 4(b), the T dependence of the inter-impurity susceptibility $\chi_{12}(\omega = 0)$ is shown for $k_0R = 10$ and various values of μ. We observe that, as β increases, χ_{12} becomes strongly enhanced for $\mu = 0.1$, while it remains weak for $\mu = 0.3$. At $\mu = -0.2$, χ_{12} is antiferromagnetic for this value of k_0R. Figures 3 and 4 show that long-range FM correlations develop between the impurities depending on the position of μ.

In the QMC simulations, we find that $\langle M_1^z M_2^z\rangle$ has larger error bars when IBS is occupied. This might be due to the cancellation of the host spin polarizations originating from the split-off state and from the valence band. The intra-impurity measurements such as $\langle (M_1^z)^2\rangle$ or $G_{ii}^{\sigma}(\tau)$ do not exhibit such behavior.

Within HF, the range ξ of the FM correlations between the impurities is determined by the energy of the IBS and, hence, the energy of the split-off state: $\xi \approx (16\pi\rho_0\omega_{BS})^{-1/2}$ for a constant density of states and semi-infinite host bands. In particular, the spatial extent of the spin polarization of the valence band around the impurity is given by $4\rho_0\Delta Z_d e^{-r/\xi}/(r/\xi)$, where Z_d is the weight of the pole at ω_{BS} in the impurity single-particle Green's function. Within HF, ω_{BS} decreases rapidly as $\Delta/\Delta_G \to 0$, which agrees with the Δ dependence of the range seen in Figs. 2(a)-(c). In addition, for $T = 0$, $\Delta = 1.0$, and $0 < \mu < \omega_{BS}$, HF yields $\omega_{BS} \approx 0.02$ and $k_0\xi \approx 9$. We note that the effects of the inter-impurity correlations on the impurity single-particle Green's function are neglected within this approximation.

In the QMC and HF calculations, the location of the Fermi level with respect to the IBS is important; the FM correlations weaken as the IBS becomes occupied. Photoemission and optical measurements on $Ga_{1-x}Mn_xAs$ provide evidence that the occupation of the Mn-induced impurity band is similarly important for the magnetic properties of this prototypical DMS ferromagnet. Photoemission experiments [14] observed an Mn-induced state above the valence band and right below the Fermi level in $Ga_{1-x}Mn_xAs$. Clearly, inverse photoemission experiments are required to detect the unoccupied portion of the Mn-induced impurity band. STM experiments also observed the impurity band in this compound [15]. Recent optical-absorption measurements [16], which show a redshift of the mid-infrared peak with Mn doping, provide evidence that the Fermi level is located in the Mn-induced impurity band in $Ga_{1-x}Mn_xAs$. Furthermore, as the impurity band becomes less occupied with Mn doping, the Curie temperature T_c increases in annealed samples, which is in agreement with the QMC and HF results. The comparisons of these experiments and the numerical results suggest that the Anderson Hamiltonian for a semiconductor host provides a basic electronic model for the DMS ferromagnets.

These numerical results also suggest that, in addition to Mn substitution, a possible way of increasing T_c in $Ga_{1-x}Mn_xAs$ is to decrease the impurity-band occupation by changing the semiconductor host material or by using additional dopants. Alternative ways of enhancing the FM correlations in this model is provided by varying the hybridization parameter Δ or the semiconductor gap Δ_G. The QMC simulations show that ξ increases as Δ goes from 4.0 to 1.0. Within HF, ξ can take very large values as Δ/Δ_G decreases. Recently, T_c's exceeding the room temperature have been reported in dilute oxides such as ZnO and TiO_2 with transition metal impurities [17, 18]. At this point, it is important to determine whether the Anderson model of a magnetic impurity applies to this case. Obviously, experiments probing the electronic state of the FM dilute oxides are necessary to answer this question.

The two-impurity Anderson model for a semiconductor host might be oversimplified for describing the ferromagnetism of the DMS. Our calculations are for spin-1/2 Anderson impurities, and we have neglected the multi-orbital structure of the spin-5/2 Mn impurities. Hence, the effects of the atomic Hund's rule couplings are not included. In addition, we neglect the long-range Coulomb repulsion between the impurity and the host electrons. Keeping these caveats in mind, it is interesting to note that the theoretical studies of high-T_c DMS ferromagnetism could have preceded the experimental discovery, if the Hirsch-Fye algorithm had been applied to a semiconductor host when it was developed twenty years ago.

In summary, we have presented QMC results to show that long-range FM correlations develop between magnetic impurities in semiconductors. In particular, the FM correlations have the longest range when the Fermi level is located above the top of the valence band, and they weaken as the IBS becomes occupied. Hence, the position of the Fermi level with respect to the IBS plays a crucial role in determining the range of the FM correlations in agreement with HF. Comparisons with the photoemission and optical absorption experiments suggest that the two-impurity Anderson model in a semiconductor host captures the basic electronic structure of $Ga_{1-x}Mn_xAs$. The numerical results presented here outline the parameter regime which yields the longest-range FM correlations, and this information might be useful for synthesizing higher-T_c DMS materials.

We thank V.A. Ivanov for bringing Ref. [7] to our attention and for useful comments. This work was supported by the NAREGI Nanoscience Project and a Grant-in Aid for Scientific Research from the Ministry of Education, Culture, Sports, Science and Technology of Japan, and NEDO. One of us (N.B.) gratefully acknowledges support from the Japan Society for the Promotion of Science and the Turkish Academy of Sciences (EA-TUBA-GEBIP/2001-1-1).

[1] *Concepts in Spin Electronics*, edited by S. Maekawa (Oxford Univ. Press, 2006).
[2] H. Ohno *et al.*, Phys. Rev. Lett. **68**, 2664 (1992); Appl. Phys. Lett. **69**, 363 (1996).
[3] I. Žutić, J. Fabian, and S. Das Sarma, Rev. Mod. Phys. **76** 323 (2004).
[4] F.D.M. Haldane and P.W. Anderson, Phys. Rev. B **13**, 2553 (1976).
[5] M. Ichimura, K. Tanikawa, S. Takahashi, G. Baskaran, and S. Maekawa, *Foundations of Quantum Mechanics in the Light of New Technology* (ISOM-Tokyo 2005), edited by S. Ishioka and K. Fujikawa, (World Scientific, Singapore, 2006), 183-186.
[6] K. Tanikawa, S. Takahashi, M. Ichimura, G. Baskaran, and S. Maekawa, preprint.
[7] P.M. Krstajić, V.A. Ivanov, F.M. Peeters, V. Fleurov, and K. Kikoin, Europhys. Lett. **61**, 235 (2003).
[8] K. Yamauchi, H. Maebashi, and H. Katayama-Yoshida, J. Phys. Soc. Jpn. **72**, 2029 (2003).
[9] K. Tanikawa, N. Bulut, S. Takahashi, and S. Maekawa, unpublished.
[10] J.E. Hirsch and R.M. Fye, Phys. Rev. Lett. **56**, 2521 (1986).
[11] R. M. Fye, J.E. Hirsch, and D.J. Scalapino, Phys. Rev. B **35**, 4901 (1987).
[12] R. M. Fye and J.E. Hirsch, Phys. Rev. B **38**, 433 (1988).
[13] W. von der Linden, Appl. Phys. A **60**, 155 (1995).
[14] J. Okabayashi *et al.*, Phys. Rev. B **64**, 125304 (2001).
[15] A.M. Yakunin *et al.*, Phys. Rev. Lett. **92**, 216806 (2004).
[16] K.S. Burch *et al.*, Phys. Rev. Lett. **97**, 087208 (2006).
[17] Y. Matsumoto *et al.*, Science **291**, 854 (2001).
[18] P. Sharma *et al.*, Nature Mater. **2**, 673 (2003).